RGNZ/MGPB

Influence of Swelling on Shear Strength of Shale-Limestone Interface

Rudarsko-geološko-naftni zbornik
(The Mining-Geology-Petroleum Engineering Bulletin)
UDC: 551.2; 551.3
DOI: 10.17794/rgn.2022.5.7

Original scientific paper

Mohamed Y. Abd El-Latif[1], Tahia Awad[2] and Rasha Aly[3]

[1] *Assistant Professor, Structural Engineering Dept., Ain Shams University, P.O. Box 11517, Cairo, Egypt. mohamed.youssef@eng.asu.edu.eg, https://orcid.org/0000-0003-3547-9587*

[2] *Professor, Structural Engineering Dept., Ain Shams University, P.O. Box 11517, Cairo, Egypt, tahiaawad@hotmail.com, https://orcid.org/0000-0002-0515-0855*

[3] *Housing and Building National Research Centre 87 Tahrir St, P.O. Box 1770, El-Giza, Egypt, khalid_mansur1970@yahoo.com*

Abstract

Rock slope stability is almost controlled by the behaviour of the interface between rock layers. The presence of shale layers between limestone layers complicates this behaviour. As the shale layer undergoes swelling with moisture, it causes the shear interface properties to change with a specific behaviour different from the dry state. The behaviour will depend on the shale's degree of saturation, swelling percentage, and stress level over shale. An experimental program was carried out to determine the shear interface behaviour parameters of shale-limestone during swelling phenomena to guide stability checks. The interface cohesion and friction angle results are reported along the swelling process and compared with the dry state condition. These results help engineers assign adequate and accurate values for joint shear and normal stiffness in jointed rock slopes, including swelling layers.

Keywords:

interface; shale; rock slope; shear strength; swelling

1. Introduction

The stability of rock masses depends on the properties of intact rock, geometry, and properties of discontinuities. The shear strength of bedding planes in layered sedimentary rock masses plays a vital role in controlling the stability of slopes in these rock masses. This role is highly significant when bedding planes have a dip downslope angle towards the cliff, as they can form surfaces upon which sliding occurs. Water leaking from drainage utilities, plant irrigation, and humidity flocculation can reach these bedding planes through rock discontinuities and affect their shear strength, causing rockslides (**Protosenya and Vilner, 2022; Puzrin, 2021; Yanuardian et al., 2020**). Mokattam Plateau in Egypt is an example of hazardous rock slopes surrounded by high population densities.

Many fatal accidents in the last years happened in the Mokattam Zone due to rockfalls on humans and buildings. Although limestone formations are strong enough as intact rock, the presence of shale layers intercalated within Mokattam slopes causes many instability problems when subjected to leakage or earthquakes. On some slopes, the shale bedding layer is slightly inclined to the cliff direction (**Awad, 1997; El-Nahhas, 1990**). Comprehensive studies on rock discontinuities of Mokattam slopes showed that the most critical parameter for the slope rock matrix is the joint shear stiffness (Jks) of the bedding surface (shale-limestone joint). Therefore, it is recommended to carry out laboratory programs to investigate the interface properties of different slope materials with each other in case of various subjected stresses and water content (**Abdel Latif, 2012; Wang et al., 2020**).

Bedding plane shear stiffness is affected by rock surface roughness, overburden pressure, interface friction angle, interface cohesion, and other factors (**Zuo et al., 2020**). The main problem during the wetting and swelling of shale is that the bedding shear strength varies with swelling (**Ikechukwu et al., 2021; Rahman et al., 2018**). This variation in strength will directly affect the bearing resistance of the bedding layer and the joint shear stiffness of the bedding plane (**El-Sohby et al., 2004; Fernandez et al., 2022**). Accordingly, it affects the definition of material models in rock slope stability analyses, and in some cases, strain softening can happen after swelling (**Al-Obaydi et al., 2021; Renani and Martin, 2020; Hegazy et al., 2019; Zeng et al., 2020**). An experimental program is carried out in this research to determine the shear behaviour and parameters of the shale-limestone interface along the swelling phenomena of shale. In addition, the effect of limestone layer stress and swelling duration on the interface behaviour is considered.

Corresponding author: Mohamed Y. Abd El-Latif
e-mail address: mohamed.youssef@eng.asu.edu.eg

1.1 Geomorphology and Stratigraphy of El-Mokattam Plateau

The Mokattam upper plateau is 200 m above sea level and is capped with intercalated layers of limestone and sandstone with a thickness ranging from 9 to 11 m. Overlaying intercalated layers of shale with thickness range from 4.5 to 7.5 m and lie at 11 to 13 m depth from the ground surface as shown in **Table 1**. The upper plateau is generally less resistant to erosion and forms recessive slopes. The dip angle of exposed rocks has a gentle northeast ward of about 3°.

Table 1: Stratigraphic sections of Mokattam City **(Helmy, 1996)**

Bore hole	Description	Depth (m)
B-1	Yellowish sandy dolomitic, fossiliferous, limestone	0–10.3
	Yellowish gray expansive clay (shale) intercalated with gypsum and limestone	10.3–16.3
	Yellowish to brown calcareous silty sand	16.3–20.8
	Brownish yellow marly expansive clay (shale)	20.8–24
B-2	Yellowish sandy dolomitic, fossiliferous, limestone	0–9
	Brownish yellow marly clay with ferruginous bands	9–14
	Yellowish intercalated with marl and expansive clay (shale)	14–24
B-3	Yellowish to yellowish brown dolomitic fossiliferous limestone intercalated with vuggy sandy fossiliferous limestone	0–10
	Yellowish gray expansive clay (shale) intercalated with gypsum, hematite, sediments, and lenses of anhydrite	10–19
	Gray to white greenish expansive clay with gypsum	19–22

2. Experimental program

In this research, undisturbed samples of shale and limestone are collected from cut slopes in the Mokattam Plateau. Geotechnical properties of shale and limestone are determined and classified by different methods. The shale samples are cut to size and tested in a one-dimensional oedometer and direct shear box using a load-swell method. The shear parameters of the shale-limestone interface are determined during swelling using a direct shear test.

Shear strength is tested in a direct shear apparatus for shale and shale-limestone interface. Shear parameters are reported in case of dry condition, final swelling, and intermediate swelling ratios considering various vertical stresses. The specimens' dimensions in the shear box are (6 cm x 6 cm x 2 cm) in the case of shale only, and the dimensions are (6 cm x 6 cm x 1cm) for both limestone and shale specimens in which the bottom specimen is limestone. All samples are tested at a constant displacement rate of 0.4 mm/min. Specimens are submerged in the shear box with distilled water. Each sample is left to reach its maximum final swelling under a specific load in

Table 2: Experimental program using direct shear test

Group No	Test no	Studying factor	Normal stress (MPa)	Percent of final Swelling duration (%)	Sample thickness (cm)	Sample type
G1	1-1	Dry shale shear parameters	55	0 (dry)	2 cm	Shale
	1-2		108			
	1-3		431			
G2	2-1	Saturated shale shear parameters	14	100%	2 cm	Shale
	2-2		27			
	2-3		55			
	2-4		108			
G3	3-1	Shale-limestone shear parameters at different swelling duration	55	0 (dry)	1 cm shale + 1 cm limestone	Shale-limestone interface
	3-2			30%		
	3-3			60%		
	3-4			100%		
G4	4-1		108	0 (dry)	1 cm shale + 1 cm limestone	
	4-2			30%		
	4-3			60%		
	4-4			100%		
G5	5-1		431	0 (dry)	1 cm shale + 1 cm limestone	
	5-2			30%		
	5-3			60%		
	5-4			100%		

Table 3: Geotechnical properties of shale

Soil Properties	Shale specimen
Unit weight (kN/m^3)	19.5
Natural water content (%)	7.0
Clay content (%)	94
Liquid limit (%)	97.6
Plastic limit (%)	33
Plasticity index (%)	64.6
Shrinkage limit (%)	14.6
Free swell (%)	230
Activity= %PI / (CC-5) (**Carter and Bentley, 1991**)	0.73
Initial void ratio	0.33

the shearing box, and then it was sheared to investigate the shear properties of shale specimens during the swelling process.

The duration for reaching the maximum final swelling is reported. Then the test is repeated with another specimen having the same properties and applied stress but at an assumed duration less than the final reported duration. These assumed durations are suggested to be a ratio of 30% and 60% of the final reported duration at maximum swelling. Accordingly, testing groups are carried out to determine the shale-limestone interface properties, including testing of the shear interface at the dry state, final swelling state, and two intermediate ratios of swelling durations which are 30 and 60% of the final swelling duration. Also, the influence of vertical stress on swelling potential and shear behaviour is reported. The experimental program consists of five groups as shown in **Table 2**.

3. Results

3.1. Swelling properties of shale

The swelling and geotechnical properties of shale are summarized in **Table 3**. A free swell test is carried out on shale according to **Holtz and Gibbs (1956)** and revealed a value of about 230%. Shale activity is classified high according to **Skempton classification (1953)**. The clay mineral of the shale is montmorillonite, following the Casagrande chart as shown in **Figure 1**. Shale is considered very high swelling, and its swelling potential is 25% according to **Seed et al. classification (1960)** and modified by **Carter and Bentley (1991)**, as shown in **Figure 2**.

3.2. Compressive strength of limestone

A Universal Machine is used to obtain the limestone's unconfined compressive strength. **Figure 3** shows the failure mode of limestone. The stress-strain relationship is shown in **Figure 4.** The result shows that the maxi-

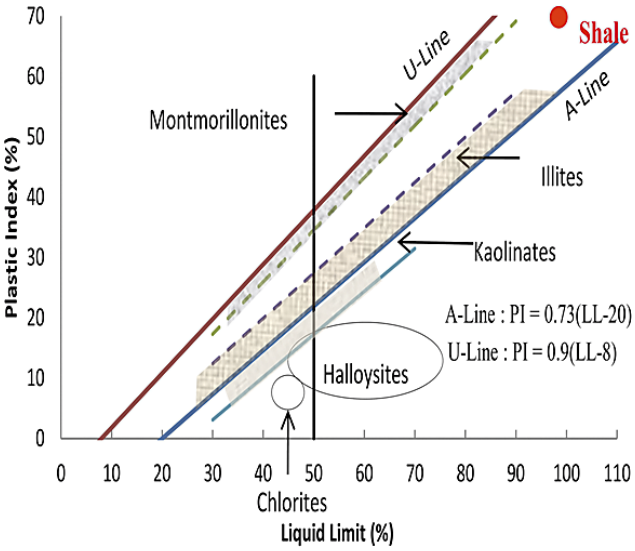

Figure 1: Classification of shale minerals using Casagrande's chart

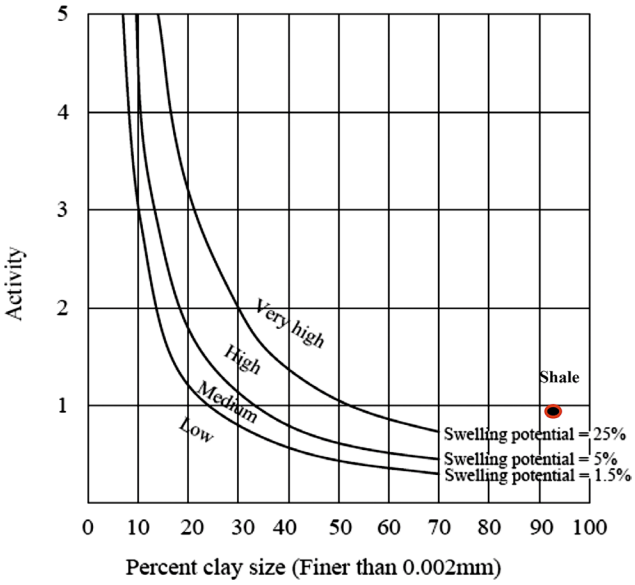

Figure 2: Classification of shale according to **Carter and Bentley (1991)**

Figure 3: Photos of failure for a limestone sample using a Universal Machine

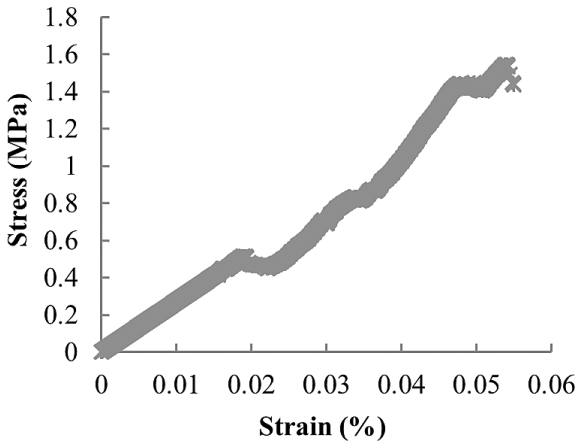

Figure 4: Stress-strain curve for the limestone sample using a Universal Machine

mum compressive strength of limestone is equal to 1.54 MPa, and the strength is moderate according to **Bell classification (1992)**.

3.3. Direct shear test results

3.3.1. Shear behaviour of shale and shale-limestone interface at dry state

The relationship between shear stress and horizontal displacement for shale and shale-limestone interface at the dry state is reported and presented. The relationship is drawn for three different normal stresses, representing the stresses induced by limestone blocks' height over the shale bedding layer. **Figure 5** shows the relation for shale only, while **Figure 6** shows the relation for the shale-limestone interface. The figures show that the shear stress of the interface plane is about half that of pure shale, and the shale is undergoing a gradual strain weakening which may cause post-failure dilation. It can be noted that shale represents different peak and residual stresses. Shale-limestone interface is undergoing perfect strain plasticity, which will minimize the deviatory dilation and represent the same value for peak and residual stresses.

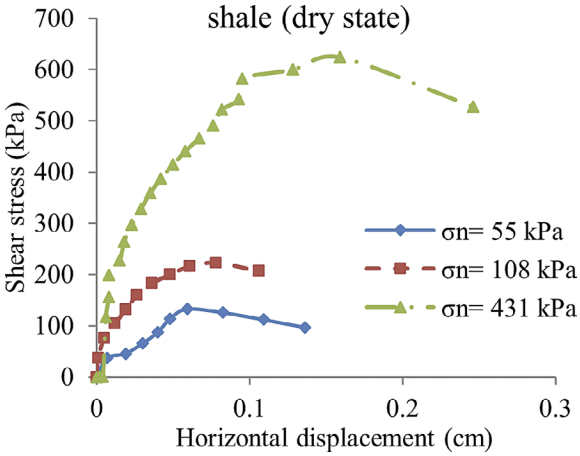

Figure 5: Shear stress versus horizontal displacement for shale in the dry state

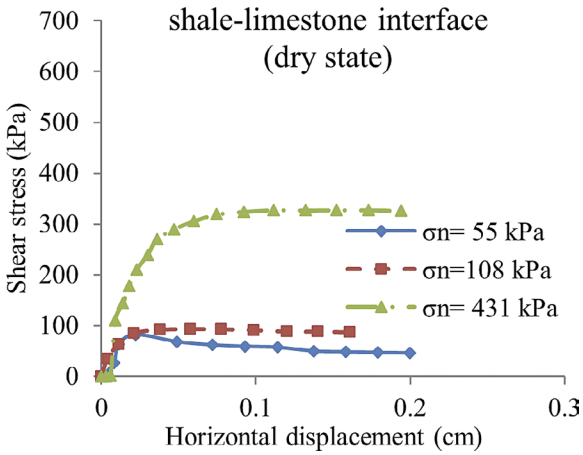

Figure 6: Shear stress versus horizontal displacement for shale-limestone interface in the dry state

3.3.2. Shear behaviour of shale and shale-limestone interface at final swelling

Shale specimens are subjected to different normal stresses to investigate the shear behaviour of shale after swelling. Each specimen is subjected to a specific stress, wetted, and left saturated until it reaches its final swelling potential. The relationship between shear stress and horizontal displacement for shale and shale-limestone interface at the final swelling state is reported and presented. **Figure 7** shows the relation for shale only, while **Figure 8** shows the relation for the shale-limestone interface. The figures show that the shear stress of the interface is about half that of shale. And both undergo strain plasticity, which decreases the deviatory dilation and represents the same value for peak and residual stresses. The measured water content at final swelling was about 26%.

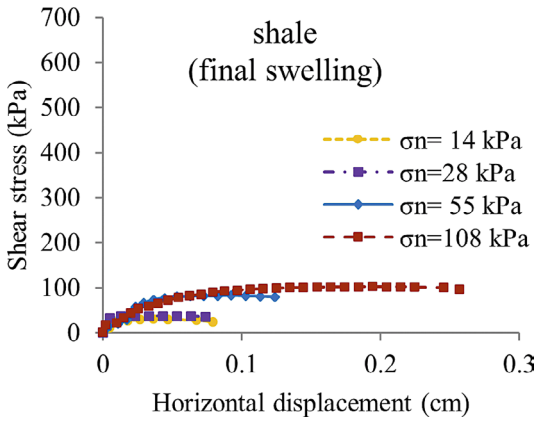

Figure 7: Shear stress versus horizontal displacement for shale at final swelling state

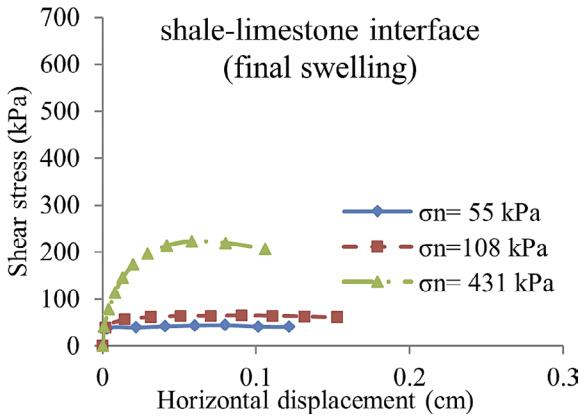

Figure 8: Shear stress versus horizontal displacement for shale-limestone interface at final swelling state

3.3.3. Shear envelop of shale and shale-limestone interface

The shear envelopes for dry and final swelling states for shale and shale-limestone interface are shown in **Figures 9** and **10**, respectively. **Figures 11** and **12** compare

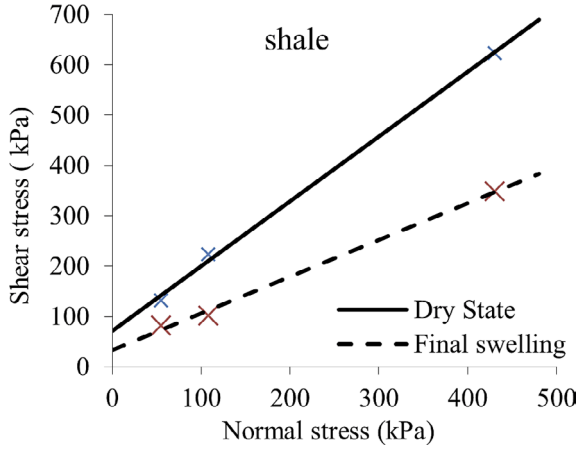

Figure 9: Shear strength envelope at dry state and final swelling state

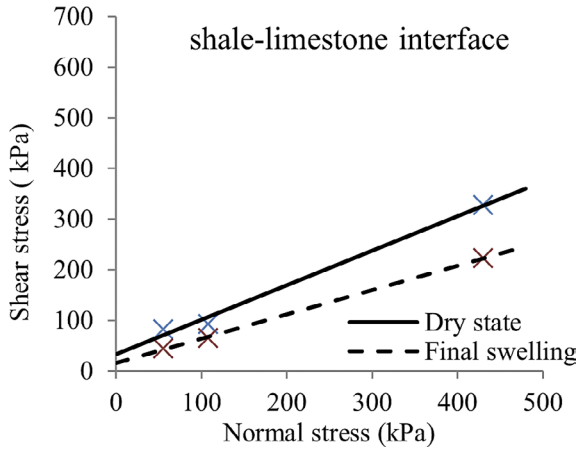

Figure 10: Shear strength envelope at dry and final swelling state

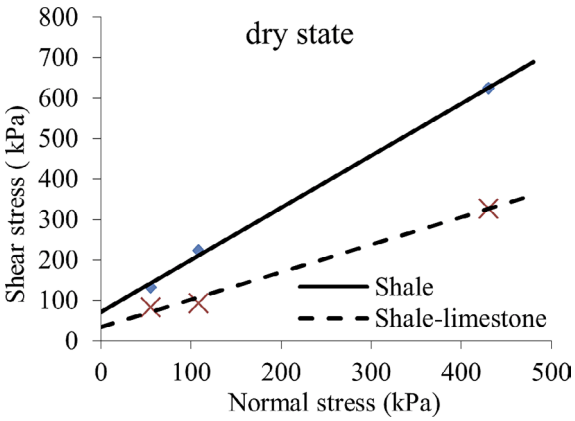

Figure 11: Shear strength envelope at dry state

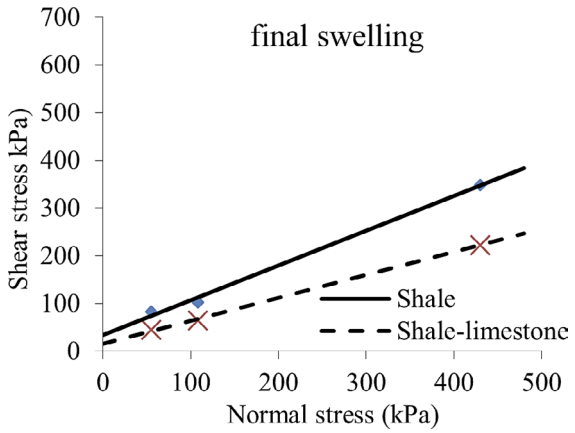

Figure 12: Shear strength envelope at final swelling state

Table 4: Maximum shear stress at different normal stresses

Normal stress (kPa)	Maximum shear stress τ_{max} (kPa)			
	Shale		Shale-limestone interface	
	Dry	Final swelling	Dry	Final swelling
55	132.39	82.57	82.38	44.13
108	223.00	101.99	93.16	64.72
431	623.70	348.14	327.54	222.61

the shear envelopes of shale and shale limestone interface in the two states. The maximum shear stress values are presented in **Table 4**. The failure envelopes and maximum shear stress values show that a significant decrease happened due to the swelling of shale. This decrease appears on the shear parameter values. **Table 5** represents the values of shear strength parameters at dry and final swelling states. The ratio between saturated and dry shear parameters is calculated and summarized in **Table 6** to determine the percentage of weakness due to swelling. The effect of limestone height on the interface maximum shear stress is shown in **Figure 13**.

The results show that the maximum shear stress of shale-limestone interface is less than that for shale at dry

Table 5: Shear strength parameters at dry and final swelling state

State	Shale		Shale-limestone interface		C_a/ C	δ/ ø
	Cohesion (C kPa)	Angle of shear resistance (Ø)	Interface cohesion (C_a kPa)	Interface friction angle (δ)		
Dry soil	C_d = 70.61	$Ø_d$ = 51.1	C_{ad} =33.34	$δ_d$ =33.54	0.513	0.65
Final swelling	C_s = 23.44	$Ø_s$= 36.95	C_{as}= 11.77	$δ_s$ =25.4	0.5	0.68

where C is the cohesion of shale, C_d represents cohesion at dry state for shale, C_s is the cohesion at final swelling state for shale, C_a is the shale-limestone interface cohesion, C_{ad} is shale-limestone interface cohesion at dry state, C_{as} is shale-limestone interface cohesion at final swelling state, Ø is angle of shear resistance, $Ø_d$ is angle of shear resistance at dry state for shale, $Ø_s$ is angle of shear resistance at final swelling for shale, δ is shale-limestone interface friction angle, $δ_d$ is shale-limestone interface friction angle at dry state, and $δ_s$ is shale-limestone interface friction angle at final swelling state.

and final swelling state. This result matches the planes of failure which occurred in Mokattam and explains the reason for failure on these planes (**Elleboudy et al., 2015**). The interface maximum shear stress is about 60% of that of shale. The readings show that interface cohesion is about half the cohesion of shale in the dry and final swelling states. The interface friction angle is about two-thirds of shale in the two cases. A significant decrease happens in shale and interface shear parameters due to swelling. The results show that the cohesion decreases to a third of its dry value, and the friction loses a quarter of its value.

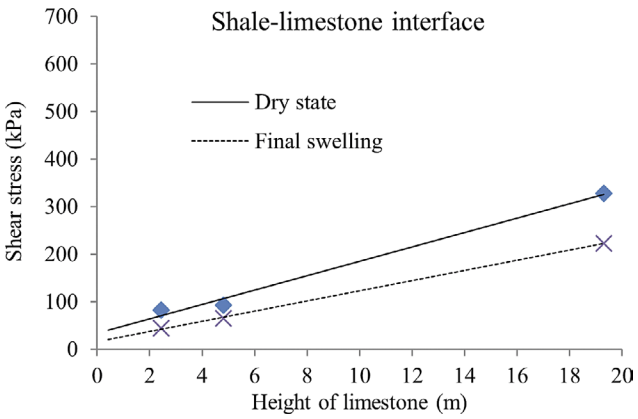

Figure 13: Maximum shear stress versus height of limestone over shale bedding layer (shale-limestone interface)

Table 6: Shear parameters ratio (saturation/dry)

Shear parameter ratio	Shale		Shale-limestone interface	
	C_s/ C_d	$Ø_s$/ $Ø_d$	C_{as}/ C_{ad}	$δ_s$ / $δ_d$
(Saturation/dry) ratio	0.33	0.72	0.35	0.76

4. Discussion

The effect of swelling duration on the relation of shear stress versus horizontal displacement of shale-limestone interface for different normal stresses is shown in **Figures 14** to **16**. Shear strength envelopes of shale-limestone interface at different swelling durations are shown in **Figure 17**. **Table 7** summarizes the values of maximum shear stress at different swelling durations and limestone heights. Shale-limestone interface shear parameters at different swelling durations are presented in **Table 8**, and the ratio of these parameters values to the dry values are calculated for different swelling durations.

The results show that the shear parameters decrease as the swelling duration increase. The shear envelopes of swelling durations are close to each other with the same friction angle than that of the dry state. Significant change happens in cohesion due to swelling, while friction appears constant during swelling. The interface cohesion decreases with swelling until it reaches 35% of its dry value. The interface friction angle decreased sud-

Table 7: Maximum shear stress results for shale-limestone interface at different swelling durations

Normal stress σn (kPa)	Height of limestone (m)	Maximum shear stress (kPa) shale-limestone interface			
		Dry state	30% swelling duration	60% swelling duration	100% swelling duration
55	2.43	82.38	58.84	51.98	44.13
108	4.82	93.16	80.41	68.65	64.72
431	19.3	327.54	239.77	237.32	222.61

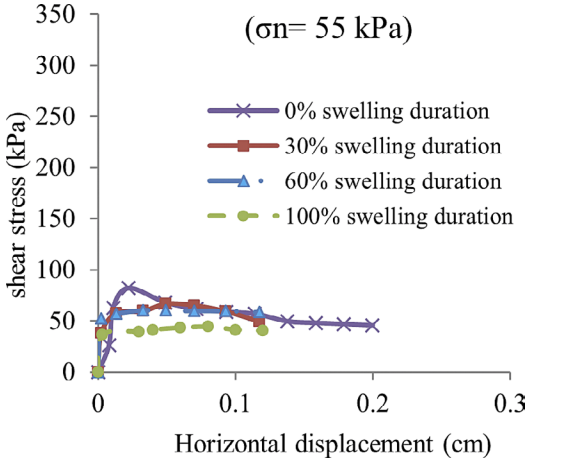

Figure 14: Shear stress versus horizontal displacement for shale-limestone interface at different swelling durations (normal stress= 0.56 kg/cm²)

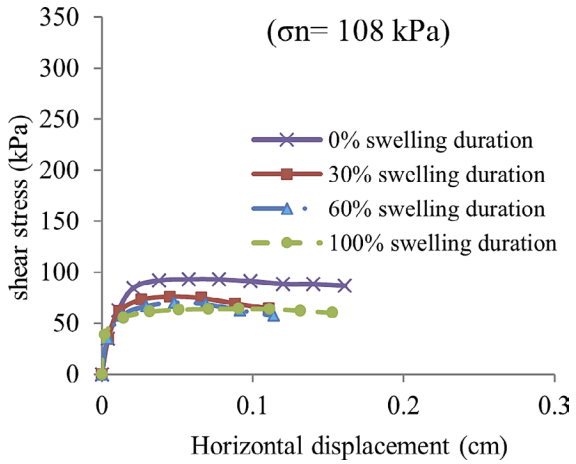

Figure 15: Shear stress versus horizontal displacement for shale-limestone interface at different swelling durations (normal stress= 1.1 kg/cm²)

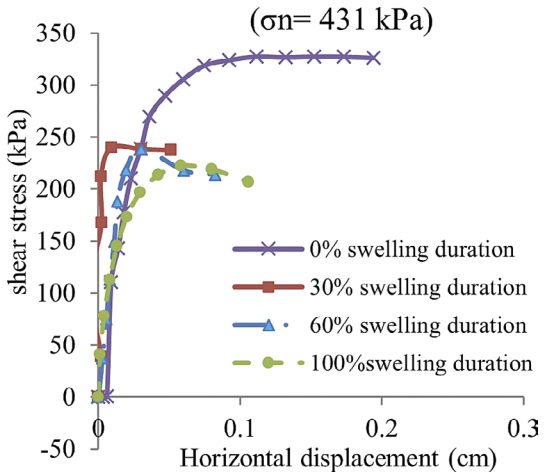

Figure 16: Shear stress versus horizontal displacement for shale-limestone interface at different swelling durations (normal stress= 4.4 kg/cm²)

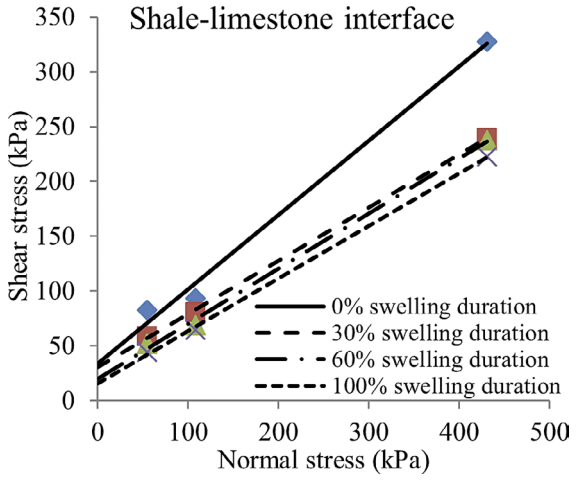

Figure 17: Shear strength envelope for shale-limestone interface at different swelling durations

denly with swelling to 75% of its dry value and remains constant during the swelling process.

Table 8: Shale-limestone interface shear parameters at different swelling durations

Swelling duration %	Interface cohesion (Ca kPa)	Interface friction angle (δ)	Ca saturated / Ca dry	δ saturated / δ dry
0% (Dry)	33.34	33.7	-	-
30%	28.44	25.96	0.85	0.77
60%	18.63	26.6	0.59	0.79
100% (Final)	11.77	25.4	0.35	0.75

5. Conclusions

The experimental results indicate that the shear parameters of shale-limestone interface are affected by the swelling process, duration of swelling, and limestone stress. The maximum shear stress of shale-limestone interface is less than that for shale at dry and final swelling states. This result matches the plane of failure in Mokattam and explains the failure on this plane. The interface maximum shear stress is about 60% of that of shale. The interface maximum shear stress and shale cohesion in case of the final swelling state are less than that in the dry state by about 32–46% and 67%, respectively. The angle of shear resistance for shale in case of maximum swelling is less than that in dry conditions by about 28%.

The interface cohesion of shale-limestone is less than that of shale by about 50%. The interface angle of shear resistance of shale-limestone is less than that of shale by about 35%. The shale-limestone interface shear parameters decrease as the swelling duration increases. The interface cohesion decreases with swelling until it reaches 35% of its dry value. The interface friction angle decreases suddenly with swelling to 75% of its dry value and remains constant during the swelling process. The interface maximum shear stress of shale-limestone increases with the increase of the height of the limestone layer. Based on these results, more accurate values can be estimated for joints shear (Jks) and normal stiffness (Jkn).

Conflict of interest

We wish to confirm that there are no known conflicts of interest associated with this publication and there has been no significant financial support for this work that could have influenced its outcome.

6. References

Abdel Latif, M. (2012): Slope stability of jointed rock masses. Faculty of Engineering, Ain Shams University, 274 p.

Al-Obaydi, M. A., Al-Kiki, I. M., and Aldaood, A. H. (2021): Effect of swelling on the shear strength behaviour of expansive soil. International Journal of Geotechnical Engineering, 15, 8. https://doi.org/10.1080/19386362.2019.1651043

Awad, T. (1997): Geotechnical Characteristics of Clay stone Formations of Gebel Mokattam Egypt. Third Alexandria Conference on Structure and Geotechnical Engineering, 12.

Carter, M., and Bentley, S. (1991): Correlation of soil properties. Pentech Press Publishers, London, 130 p.

Elleboudy, A. M., Winter, M. G., Smith, D. M., Eldred, P. J. L. and Toll, D. G. (2015): Investigating rock-slope failures East of Cairo. In Geotechnical Engineering for Infrastructure and Development, 1537–1542. https://doi.org/10.1680/ecsmge.60678.vol4.225

El-Nahhas. (1990): Geotechnical characteristics of limestone formations of Gebel Mokattam area. First Alexandria Conf. on Structure and Geotechnical Engineering, 10.

El-Sohby, M., Mazen, S., and Aboushook, M. (2004): Slope degradation and analysis of Mokattam Plateau, Egypt. 2nd International Conference on Geotechnical Site Characterization (ISC-2), Porto, 1081–1887.

Helmy, H. (1996). Stability analysis of jointed rock slopes with special application on Mokattam. Faculty of Engineering, Ain Shams University, 104 p.

Ikechukwu, A. F., Hassan, M. M., and Moubarak, A. (2021): Swelling stress effects on shear strength resistance of subgrades. International Journal of Geotechnical Engineering, 15, 8. https://doi.org/10.1080/19386362.2019.1656445

Fernandez, J. C. J., Jano, L. C., Alonso, A. G., Fernandez, E. B., Fernandez, J. C. G., Gonzalez, V. C., Fresno, D. C., and Sanchez, D. G. (2022): 3D numerical simulation of slope-flexible system interaction using a mixed FEM-SPH model. Ain Shams Engineering Journal, 13, 2, 21. https://doi.org/10.1016/j.asej.2021.09.019

Protosenya, A., and Vilner, M. (2022): Assessment of excavation intersections' stability in jointed rock masses using the discontinuum approach. Rudarsko-Geološko-Naftni Zbornik, 37, 2, 137–147. https://doi.org/10.17794/rgn.2022.2.12

Puzrin, A. M. (2021): Landslide influence zone – a hidden hazard. Géotechnique, 71, 9, 781-794. https://doi.org/10.1680/jgeot.19.P.333

Rahman, A. S. A., Noor, M. J. M., Jais, I. B. M., Sidek, N., and Ahmad, J. (2018): Shear strength of granitic residual soil in saturated and unsaturated conditions. AIP Conference Proceedings, 10. https://doi.org/10.1063/1.5062629

Renani, H. R., and Martin, C. D. (2020): Factor of safety of strain-softening slopes. Journal of Rock Mechanics and Geotechnical Engineering, 12, 3, 473-483. https://doi.org/10.1016/j.jrmge.2019.11.004

Wang, C., Elsworth, D., Fang, Y., and Zhang, F. (2020): Influence of fracture roughness on shear strength, slip stability and permeability: A mechanistic analysis by three-dimensional digital rock modeling. Journal of Rock Mechanics and Geotechnical Engineering, 12, 4, 720–731. https://doi.org/10.1016/j.jrmge.2019.12.010

Yanuardian, A. R., Hermawan, K., Martireni, A. P., and Tohari, A. (2020): The influence of discontinuities on rock mass quality and overall stability of andesite rock slope in west java. Rudarsko-Geološko-Naftni Zbornik, 35, 3, 67–76. https://doi.org/10.17794/rgn.2020.3.7

Hegazy, Y. A., Akl, S. A., and Adel, H.A. (2019): Reliability based design of the rock side slope for upper plateau in mokattam area considering optimal cost value. Journal Of Al-Azhar University Engineering Sector, 14, 50, 15–27.

Zeng, Z., Cui, Y.-J., Conil, N., and Talandier, J. (2020): Effects of technological voids and hydration time on the hydro-mechanical behaviour of compacted bentonite/claystone mixture. Géotechnique, 72, 1, 34–47. https://doi.org/10.1680/jgeot.19.P.220

Zuo, J., Lu, J., Ghandriz, R., Wang, J., Li, Y., Zhang, X., Li, J., and Li, H. (2020): Mesoscale fracture behaviour of Longmaxi outcrop shale with different bedding angles: Experimental and numerical investigations. Journal of Rock Mechanics and Geotechnical Engineering, 12, 2, 297–309. https://doi.org/10.1016/j.jrmge.2019.11.001

SAŽETAK

Utjecaj bubrenja na smičnu čvrstoću kontaktne površine šejla i vapnenca

Stabilnost stijenskih kosina uglavnom je uvjetovana interakcijom kontaktne površine između slojeva stijenske mase. Prisutnost slojeva šejla između slojeva vapnenca usložnjava tu situaciju. Kako sloj šejla bubri zbog vlage, dolazi do promjene svojstava kontaktne površine koja se specifično razlikuje od suhoga stanja. Ponašanje će ovisiti o stupnju zasićenosti šejla, postotku bubrenja i veličini naprezanja u materijalu iznad šejla. Provedeno je eksperimentalno ispitivanje za određivanje parametara ponašanja smicanja kontaktne površine šejla i vapnenca tijekom pojave bubrenja te je provedena provjera stabilnosti. Vrijednosti kohezije i kuta unutarnjega trenja na kontaktnim površinama opažane su tijekom procesa bubrenja i uspoređivane su s vrijednostima suhoga stanja. Ti rezultati pomažu inženjerima odabrati odgovarajuće i pouzdane vrijednosti smične i normalne krutosti za diskontinuirane stijenske kosine na kojima se pojavljuju slojevi koji bubre.

Ključne riječi:
kontaktna površina, šejl, stijenska kosina, smična čvrstoća, bubrenje

Author's contribution

Rasha Aly (MSc. Eng, assistant researcher) performed the data collection, field work and analyzed the results. **Tahia Awad** (Professor Full) methodology and final revision. **Mohamed Y. Abd El-Latief** (Assistant Professor) managed the whole process from the beginning to the end, including writing.